


Novel methodology to couple decline curve analysis with CFD reservoir simulations for complex shale gas reservoirs

Syed Oubee Khadri¹ | Mohammed J. Al-Marri^{1,2} | Mustafa Nasser^{1,2} |
Fadhil Sadooni³ | Ezeddin Shirif⁴ | Ibnelwaleed A. Hussein^{1,2} 

¹Gas Processing Center, Qatar University, Doha, Qatar

²Department of Chemical Engineering, Qatar University, Doha, Qatar

³Environmental Science Center, Qatar University, Doha, Qatar

⁴Program of Petroleum Systems Engineering, University of Regina, Regina, Saskatchewan, Canada

Correspondence

Ibnelwaleed A. Hussein, Gas Processing Center, Qatar University, Doha, Qatar.
Email: ihussein@qu.edu.qa

Mohammed J. Al-Marri, Department of Chemical Engineering, Qatar University, Doha, Qatar.
Email: m.almarri@qu.edu.qa

Funding information

Qatar National Research Fund, Grant/Award Numbers: NPRP12S-0130-190023, NPRP12S-0305-190235

Abstract

Shale reservoirs are highly complex and are difficult to study using conventional reservoir simulation tools. This study introduces a novel methodology for estimating production from complex shale gas reservoirs by coupling decline curve analysis (DCA) with computational fluid dynamics (CFD) simulations. The proposed method uses exponential DCA to analyze production data from a dual porosity–permeability shale gas transport model. These complexities include fracture characteristics, geomechanical properties, nanopore confinement effects, and multiple flow mechanisms contributing to the total production performance. The shale gas transport model is validated through historical production data from Marcellus shale. The new methodology also tests fracture characteristics. It shows that increased porosity and permeability will increase the recoverable reserves but will have varying effects on the decline rate. The paper demonstrates the advantages of the proposed methodology over conventional reservoir simulation tools. It provides insights into the factors affecting shale gas production performance through the inclusion of the complexities of an unconventional shale gas reservoir. The paper provides a proof of concept on the particular reservoir of which the field data is provided—Barnett and Marcellus Shale.

KEYWORDS

computational fluid dynamics, declining curve analysis, flow in porous media, gas production, gas reservoirs, shales

1 | INTRODUCTION

Shale gas reservoirs are unconventional hydrocarbon resources that have become increasingly important due to advancements in hydraulic fracturing and horizontal drilling technologies.^[1] The shift towards unconventional resources is observed globally, notably in the USA, China,

Russia, Canada, and others.^[2] These technologies have made it possible to extract hydrocarbons from shale formations that were previously uneconomical to produce. The oil and gas industry focuses on these unconventional reservoirs due to their abundance and lower overall expenditure.^[3]

Shale gas reservoirs are known for their complexity due to several factors, such as the presence of nanopores,

This is an open access article under the terms of the [Creative Commons Attribution](https://creativecommons.org/licenses/by/4.0/) License, which permits use, distribution and reproduction in any medium, provided the original work is properly cited.

© 2024 The Author(s). *The Canadian Journal of Chemical Engineering* published by Wiley Periodicals LLC on behalf of Canadian Society for Chemical Engineering.

vast heterogeneity in rock morphology, and natural fractures.^[4] Due to these complexities, conventional means of reserve estimation typically underestimate or overestimate the asset. The presence of nanopores and organic matter kerogen may influence the estimation of the original gas in place as it is present as an adsorbed gas.^[5–7] Shales are characterized by very low porosity (typically less than 5%) and very low permeability (usually less than 1000 nD), which make them challenging for the recovery of economically viable hydrocarbons.^[8,9] Increased porosity is attributed to the number of natural fractures. The mode of production from organic pores would be dominated by desorption and diffusion, while diffusion is observed in inorganic pores. Furthermore, the nanoscale aspect of these types of pores does not conform to the conventional transport model defined by Darcy's law; therefore, the estimation of the production data is not accurate. The presence of natural and hydraulic fractures further adds to the complexity of the flow in these types of reservoirs.^[10] These fractures are on a micropore scale, represented by Darcy flow; however, they must be coupled to the transport model in the shale matrix to estimate production from these reservoirs accurately.

Fundamental flow mechanisms in these types of reservoirs are characterized as a non-Darcy flow regime, which is non-linear. As mentioned, diffusion (Knudsen and surface), desorption, viscous, and slip flow are dominantly observed in nanopores. The gas stored in shale reservoirs is generally determined to be either free or adsorbed. Both quantities are related to a particular flow mechanism, such as free gas being transported through the surface and Knudsen flow, and in macropores, through slip and viscous flow. In comparison, adsorbed gas turns to free gas by reducing pressure in the matrix by desorption and diffusion.^[11]

Various models are implemented, ranging from molecular simulations to provide an understanding of flow mechanisms and their weightage in the estimation of reserves, implementation of confinement effects, pore network modelling, and modifying the continuity equation by implementing different flow mechanisms and permeability correction (apparent permeability models) in the mass continuity equation.^[3,12–15] The addition of apparent permeability models and the influence of different flow mechanisms are simpler and more accurate than other proposed models in the literature. However, it is recognized that fracture–matrix interaction has associated challenges. Micheal et al.^[16] studied such interaction of both hydraulic and natural fractures with matrix by implementing a coupled dual porosity gas transport model with geomechanics of the formation by utilizing the discrete fracture model (DFM). The presence of both hydraulic and natural fractures provides a positive

effect on production performance. Real field data from reservoirs, such as Marcellus Shale and Barnett Shale, validate these models.^[16]

The complex gas transport mechanisms affect the production performance and gas reserve estimation. Decline curve analysis (DCA) is a simple and widely used technique for forecasting future production rates from historical data. Still, it has limitations when applied to shale gas reservoirs, such as assuming constant pressure and neglecting adsorption/desorption effects. Shale gas transport models (SGTM) are mathematical models that account for the physics of gas flow in shale reservoirs more accurately. Still, they require more data and computational resources than DCA.^[17] Therefore, there is a need for a method that can combine the advantages of DCA and SGTM to improve the estimation and prediction of shale gas production. Coutry et al.^[18] analyzed different DCA models on field data of Marcellus Shale to determine which are the suitable models for transient analysis. The study concluded that multiple models must be utilized to verify results.^[18]

This paper proposes a novel method that performs DCA for shale gas reservoirs using data from an SGTM developed in COMSOL. The accuracy and efficiency of the SGTM are tested using field data from Marcellus shale gas reservoirs in North America. The inclusion of DCA to conduct reserve estimation is with the injunction of current SGTM. With higher efficiency of results provided by representative SGTM, a virtual twin of a reservoir with limited ability can be utilized for DCA. The proposed methodology in the following section may assist in estimating the reserves for complex, unconventional reservoirs.

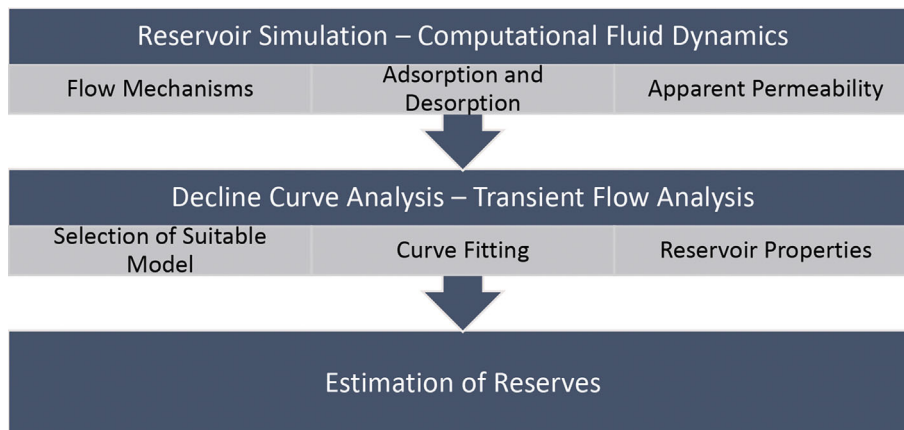
The main objectives of this study are to:

- Develop a novel methodology for reserve estimation of shale gas reservoirs using computational fluid dynamics (CFD).
- Integrate different flow mechanisms to determine shale gas reservoirs' ultimate recovery, production, and reserves.
- Conduct production analysis using the exponential DCA method.
- Investigate the influence of various reservoir parameters such as porosity, fracture, and matrix permeability on the reserve estimation.

2 | METHODOLOGY

A quantitative approach was used in this study to investigate the production performance of shale gas reservoirs. A dual porosity–permeability model is

FIGURE 1 Proposed methodology of reserve estimation through production data synthesis and rate transient analysis.



developed to simulate the gas flow and transport mechanisms in shale formations using COMSOL Multiphysics software. Field data from a shale gas reservoir in North America was used for calibration, and field data from the Marcellus shale reservoir is used for validation. Synthetic production data for different scenarios of reservoir properties and operational parameters are generated using the model. DCA is applied to the synthetic data to estimate the recoverable reserves and forecast the production rates of shale gas reservoirs. Figure 1 represents an overview of the proposed methodology in the study while also incorporating the desired results from each method (SGTM and DCA).

2.1 | Transport model for shale

SGTMs are essential in understanding flow in shale nanopores. The studies under this research segment focus mainly on the flow mechanisms occurring in these channels. These flow mechanisms directly influence the hydrocarbon recovery performance from these reservoirs while also depending on the other reservoir characteristics, such as geomechanics and pressure, volume and temperature (PVT) conditions (gas density and viscosity). Multiple models attempt to represent the reservoir performance depending on the scale of the study. However, this study will use a mass continuity equation in a DFM. Other models similar to these methodologies in the literature include dual porosity–dual permeability–local grid refinement (DP-DK-LR),^[19] equivalent continuity model (ECM),^[20] and multiple porosity model.^[21,22]

According to the study proposed by Civan et al.,^[23] DFM is extensively utilized in the fracture scale and is relatively robust compared to other models.^[23] However, it is not used for a macroscale reservoir size model, which could be attributed to the high computational power and time, with inadequate knowledge about the fracture

distribution potential and influence. Micheal et al.^[16] studied such influences through different fracture models. However, they focused on the criss-cross fracture model in general due to its more substantial impact on production.^[16]

2.1.1 | Gas apparent permeability for rock matrix and fracture based on corresponding flow mechanisms

Gas apparent permeability models are mathematical tools that describe the effective permeability of gas flow in porous media, considering the effects of gas rarefaction, gas slippage, gas sorption, and surface diffusion. These effects become significant when the pore size is comparable to or smaller than the mean free path of gas molecules, which is common in shale reservoirs. Gas apparent permeability models could be applied to pores and fractures, but they may differ in some aspects. For pores, the pore size distribution, pore shape, connectivity, and porosity are essential factors that affect the gas's apparent permeability. For fractures, the fracture aperture, roughness, tortuosity, and density are important factors that affect the apparent permeability.

Moreover, the gas flow regimes in pores and fractures may differ depending on the Knudsen number, which is defined as the ratio of the mean free path of gas molecules to the characteristic length of the flow channel. For pores, the characteristic length is usually the pore diameter, while for fractures, it is typically the fracture aperture. Therefore, different flow regimes may coexist in pores and fractures, such as viscous flow, slip flow, Knudsen diffusion, and free flow.^[24–27] The Klinkenberg gas apparent permeability model is a classical model that describes the gas flow behaviour in porous media, considering the effect of gas slippage or rarefaction. Gas slippage occurs when the pore size is comparable to

or smaller than the mean free path of gas molecules, which causes the gas molecules to collide more frequently with the pore wall than with each other. This slippage reduces the resistance to gas flow and increases the effective permeability of the porous medium. It is applied to fracture pore network to incorporate gas slippage effects in the performance of the reservoir by the following expressions^[6,16]:

$$k_f = k_{fi} \left(\frac{p_f + b_f}{p_f} \right) \quad (1)$$

where b_f is the fracture's Klinkenberg coefficient, p_f is the fracture network's pressure, k_{fi} is its intrinsic permeability, and b_f is determined by the following correlation^[28]:

$$b_f = \frac{\mu_f D_{kf}}{k_{fi}} \quad (2)$$

where μ_f is the viscosity of the gas in the crack and D_{kf} is the fracture network's Knudsen diffusion coefficient, both of which are reported by the following^[28]:

$$D_{kf} = \frac{4k_{fi} \sqrt{\varphi_f}}{2.8284 \sqrt{k_{fi}}} \cdot \sqrt{\frac{T p R}{2M}} \quad (3)$$

A similar methodology is implemented for matrix; however, the Knudsen diffusion coefficient is modified to ascertain the higher influence of the flow mechanism.^[16] The following expression defines the apparent gas permeability for the matrix:

$$k_m = k_{mi} \left(\frac{p k_{mi} + m D_m}{p k_{mi}} \right) \quad (4)$$

where k_m is the apparent gas permeability of the matrix, k_{mi} is the intrinsic permeability, mD , and D_m is the Knudsen diffusion coefficient for diffusion in the matrix. The following expression defines the diffusion coefficient:

$$D_m = \frac{4k_{mi} \sqrt{\varphi_m}}{2.81708 \sqrt{k_{mi}}} \cdot \sqrt{\frac{T \pi R}{2M}} \quad (5)$$

where M is the molar mass of methane gas, 16 g/mol.

2.1.2 | Gas viscosity and real gas expression

Shale gas transport is a complex phenomenon that involves different mechanisms, such as bulk diffusion, Knudsen diffusion, surface diffusion, and convective flow. These mechanisms are influenced by various factors such as pore size, pressure, temperature, adsorption, and real gas effect.^[3,26,29–32] The real gas effect refers to the deviation of

gas behaviour from the ideal gas law due to high-pressure and low-temperature conditions. The real gas effect affects the thermodynamic parameters of the free gas, and the adsorption and the transport capacity of the adsorbed gas.^[33,34]

One of the challenges in modelling shale gas transport is to account for the real gas effect and its impact on the effective permeability and apparent permeability of the shale matrix. Effective permeability is the intrinsic property of the porous medium that reflects its ability to transmit fluid under a given pressure gradient. Apparent permeability is the evident property of the fluid that reflects and demonstrates its ability to flow under a given pressure gradient. Both effective permeability and apparent permeability are affected by the real gas effect, as well as by gas slippage and surface diffusion. Gas slippage is the phenomenon of gas molecules slipping along the pore wall due to a low Knudsen number. Surface diffusion is the phenomenon of gas molecules diffusing along the adsorbed layer due to a concentration gradient.^[27,35,36]

Based on the findings from experimental studies,^[37,38] methane is usually confined within the tight shale formation in the form of high pressure. With the change in reservoir pressure, resulting properties also vary. Therefore, based on the real gas law,^[32,39] the pressure-dependent density is calculated by the following equation:

$$\rho_m = \frac{pM}{ZRT} \quad (6)$$

where ρ_m is the density of methane, p is the reservoir pressure, M is the molar mass of natural gas (16 g/mol), Z is the real gas compressibility factor, R is the universal gas constant (8.3142 J/K/mol), and T is the reservoir temperature. The real gas compressibility factor Z can be obtained through either equation of state, such as Peng–Robinson or Redlich–Suave. However, the explicit empirical equation for methane is utilized for this study due to its accuracy.^[40] The expression is as follows:

$$Z = (0.702e^{-2.5T_{pr}})P_{pr}^2 - (5.524e^{-2.5T_{pr}})P_{pr} + (0.044T_{pr}^2 - 0.164T_{pr} + 1.15) \quad (7)$$

where T_{pr} and P_{pr} are referred to as reduced pseudo temperature and pressure of the methane gas, respectively. The following expressions define the pseudo parameters:

$$T_{pr} = \frac{T}{T_c} \quad (8)$$

$$P_{pr} = \frac{P}{P_c} \quad (9)$$

where T_c and P_c are the critical temperature and pressure of the natural gas (methane). For single-phase methane gas, $T_c = 191\text{ K}$; $P_c = 4.64\text{ MPa}$.^[16] After defining the real gas density of methane; viscosity change is also considered in the model. However, it might cause a circular dependency on the pressure of the matrix or fracture as it is a dependent variable in the equations of continuity and mass flow. An empirical correlation proposed by Lee et al. is utilized for this model, and expressed as follows^[41]:

$$\mu = 10^{-7} K e^{X(0.001\rho_m)^Y} \quad (10)$$

where X , Y , and K are the empirical parameters and are defined by the following expressions:

$$\begin{cases} Y = 0.2X + 2.4 \\ X = 3.5 + 10M + 547.8/T \\ K = (22.7 + 48.3M)T^{1.5} / (209 + 19000M + 1.8T) \end{cases} \quad (11)$$

2.1.3 | Governing equation for gas flow in the rock matrix

SGTMs are mathematical tools that aim to predict the gas flow behaviour in shale reservoirs characterized by complex pore structures, diverse gas occurrence forms, and multiple transport mechanisms. Different models have been developed based on different assumptions, methods, and scales, such as analytical solutions,^[27] numerical simulations,^[42] and artificial intelligence methods.^[43] The main transport mechanisms that affect shale gas transport and production are viscous flow, slip flow, Knudsen diffusion, surface diffusion, free flow, adsorption, and desorption. These mechanisms depend on pore size, shape, surface type, thermal maturity, displacement pressure, and gas thermodynamics. The contribution of each mechanism varies with the effective pore diameter, the gas-wall interactions, the Knudsen number, and the gas sorption capacity. Understanding these mechanisms and their interactions is essential for accurately evaluating shale gas production and recovery.

Based on earlier studies, the shale matrix is a microporous/nanoporous medium with a large number of micro/nanopores, some of which may be smaller than 10 nm and exhibit a strong nano-confined effect.^[44–46] As a result, Darcy's law and other classical flow theories based on continuous assumptions need to be revised to accurately explain the transport behaviour of methane gas in a shale matrix. Additionally, because most methane gas is stored as an adsorption gas, the impacts of adsorption and desorption on the process of transporting gas should also be considered.^[15]

Initially, the mass continuity equation is utilized for the matrix flow. However, there are some limitations as it needs to include the flow mechanisms associated with fluid flow in shale nanopores. Therefore, by determining the processes of all the flow mechanisms by replacing the mass $c_m = c_a + c_g$ (where c_m is total concentration, c_g is the concentration of free gas, and c_a is the concentration of adsorbed gas) by its source (Knudsen diffusion and desorption)^[5,28]:

$$\nabla \cdot (\rho_m v_m) + \frac{\partial c_m}{\partial t} = q \quad (12)$$

where q represents the mass of gas moving from the matrix to the fracture, which is regarded as the source/sink of gas, and c_m stands for the concentration of gas in the matrix pores, ρ_m for the density of gas stored in the matrix, and ρ_f for the density of gas stored in the fracture. It is noted that gas is present in nanopores in adsorbed and free phases. The concentration of the adsorbed phase can be determined by the following expression^[32]:

$$c_a = \rho_{gs} \frac{V_L p}{p + p_L} (1 - \varphi) \rho_s \quad (13)$$

where V_L stands for the Langmuir volume, p for reservoir pressure, p_L for Langmuir pressure, ρ_s for standard circumstances gas density, and ρ_{gs} for shale matrix density. The equation of continuity for gas flowing in the matrix is expressed as follows^[28]:

$$\nabla \cdot (\rho_m \varphi_m) + \frac{\partial}{\partial t} \left[\rho_s \frac{V_L p}{p + p_L} (1 - \varphi) \rho_s + \rho_m \varphi_m \right] - q = 0 \quad (14)$$

For incorporating adsorption induced surface diffusion effect, the gas adsorption mass per volume is given by Micheal et al.^[16]. Equation (16) represents the final form of the gas transport mode in matrix domain.

$$q_{\text{ads}} = \frac{V_L p}{p + p_L} \frac{\rho_m M}{V_{\text{std}}} \quad (15)$$

$$\begin{aligned} \frac{\partial}{\partial t} (\rho_m \varphi_m + q_{\text{ads}} (1 - \varphi_m)) + \nabla \cdot \left[\left(-\frac{\rho_m D_m}{p} - \frac{\rho_m k_{mi}}{\mu} \right) \nabla p \right] \\ = 0 \end{aligned} \quad (16)$$

2.1.4 | Governing equation for gas flow in fractures

Gas flow in fracture has a more significant influence on the production than the matrix properties.^[16] During shale gas production, the reservoir pressure continuously decreases, thus affecting the matrix and fracture properties such as

pressure. The production occurs from the organic and inorganic pores (adsorbed and free gas), and diffuses into larger channels due to pressure differences. These larger channels are fractures that comprise higher permeability. In this study, only hydraulic fractures are considered; in this case, the sink term refers to gas flow from the fracture network to the wellbore. The equation of diffusion of free gas in the fracture is provided by the following^[3,16,47]:

$$d_f \frac{\partial(\rho_m \phi_f)}{\partial t} - \nabla_T \left(-d_f \frac{\rho_m k_f}{\mu} \nabla p_f \right) = d_f Q_m \quad (17)$$

where Q_m is the source term, d_f is the fracture aperture, and p_f is the fracture reservoir pressure. The resulting source term is defined to be the difference between the gas production from the wellbore (sink) Q_p and the gas diffusion into fracture G , which the following expression can define:

$$Q_m = G - Q_p \quad (18)$$

The gas diffusion from the matrix into fracture is expressed as follows^[28]:

$$G = \frac{\rho_m \omega k_m}{\mu_f} (P_m - P_w) \quad (19)$$

$$\omega = 4 \left(\frac{L_x^2 L_y^2 + L_y^2 L_x^2}{L_x^2 L_y^2} \right) \quad (20)$$

where ω is the coefficient of flow between the matrix and fractures, and L_x and L_y are considered to be fracture spacing in the x and y directions. The expression is modified from its parent equation for 3D fractures.^[48]

2.2 | DCA-production data analysis

Exponential decline curve analysis (EDCA) is one of the empirical methods of DCA that could be used to estimate the reserves and forecast the production of shale gas reservoirs. EDCA assumes that the production rate declines exponentially with time, which means that the decline rate is constant and independent of time. EDCA is utilized when b (decline exponent of Arps equation) is considered or assumed to be 0.^[49,50] The basic equation of EDCA is as follows:

$$q_t = q_i e^{-D_i t} \quad (21)$$

where q_t is the production rate at time t , and q_i and D_i are the initial production and decline rates, respectively.

EDCA can be applied to shale gas reservoirs when the production data shows a linear trend on a semi-log

plot. EDCA is simple and easy to use, but it has some limitations. First, it may not be suitable for shale gas reservoirs with complex flow regimes and mechanisms, such as boundary-dominated flow, adsorption/desorption, and Knudsen diffusion. Second, it may not capture the long-tailed behaviour of shale gas production, so it may underestimate the reserves and overestimate the decline rate. Third, it may not account for the effects of well operation changes on shale gas production, such as pressure control and shut-in periods.

Some case studies of applying EDCA to shale gas reservoirs include that of Wang et al.,^[8] who used EDCA to analyze the production patterns of Eagle Ford shale gas wells and found that the average decline rate was 0.004 per day the average estimated ultimate recovery (EUR) was 1.5 BCF per well; and Liang et al.,^[7] who used EDCA to evaluate the EUR of Barnett and Marcellus shale gas wells under different production modes and found that controlling the BHP could increase the EUR by 10%–20% compared with the constant flow rate model. Tang et al.^[51] also used EDCA to forecast the production of shale gas wells in the Sichuan Basin, China, and found that the average decline rate was 0.003 per day and the average EUR was 0.8 BCF per well.^[51] Tan et al.^[17] further recommended EEDCA, a form of EDCA for shale gas reservoirs, for which early and late production data are available.

During this study, EDCA is applied to obtain net recoverable reserves through forecasting production until an economic limit of 1000 m³/day. This method provides a more straightforward option while also including influences of variation in the reservoir characteristics. The following equations express it:

$$G_{pdata} + \text{Reserves} = \text{EUR (TRR)} \quad (22)$$

where G_{pdata} is the cumulative production of the historical data, Reserves is the forecasted cumulative production, and N_t is the total recoverable reserves (TRR). Figure 2 depicts the method of reserve estimation employed here.

2.3 | Model development

2.3.1 | Model parameters and assumptions

The COMSOL Multiphysics platform develops the reservoir model using a partial differential equation (PDE) solver module. Fine meshing is done to increase the accuracy of results, but it increases the computational time. The fracture flow module incorporated in the tool included the equation representing gas transport in fractures. Figure 3 represents a schematic of the model prepared for both the validation and reservoir base models, while Table 1 depicts

the parameters for the base case model. The model was developed based on the following assumptions:

- Single component gas flow through fractures and pores occurs;
- The model ignores the effect of gravity and heterogeneity of the pore network;
- Geomechanics and its influence on gas transport is ignored;
- The flow process is assumed to be isothermal throughout the field life;
- Gas adsorption kinetics is assumed to obey the Langmuir curve and can achieve equilibrium at any reservoir pressure;

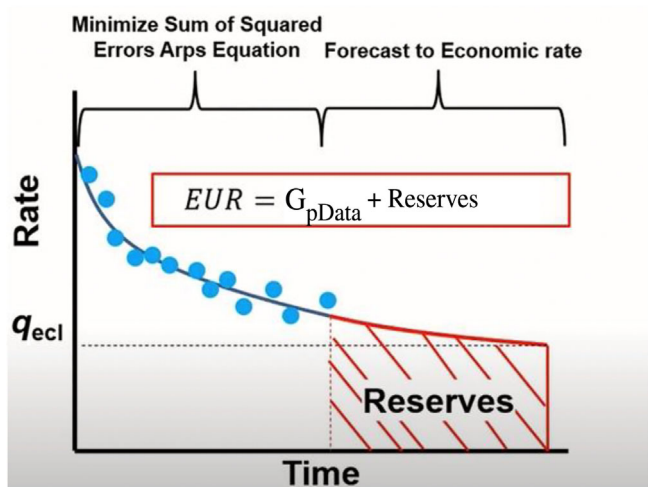


FIGURE 2 Method of determining estimated ultimate recovery (EUR) or total recoverable reserves (TRR).

- Only hydraulic fractures are considered in the simulation.^[52–55]

2.3.2 | Model meshing sensitivity

The production flow rate was used as the parameter in the mesh sensitivity analysis for the single porosity model. The sensitivity study was carried out on the parameters that define the specific mesh sizing: maximum element size, minimum element size, maximum growth rate, resolution of curvature, and resolution of narrow sections. This was done based on the parametric studies' built-in option. An overview of the instances used is given in Table 2. The findings indicate that when the maximum element size is increased, the calculation time decreases, and the results diverge from the initial findings.

Figure 4 shows Cases 1 and 3, where cumulative output with different mesh sizes yielded definitive results—while Cases 2 and 4 showed very low cumulative production since the model stops converging beyond 3000–4000 days. These outcomes lead to the use of fine mesh (case 1). The entire parametric analysis took 14.8 min on the computing machine with a 2.9 GHz Intel® Xeon® Gold 6226R CPU and 192 GB of RAM.

2.3.3 | Convergence criteria

PARDISO iterative solver was utilized for the proposed model in COMSOL, for which its M value = LU which are factors computed by the solver. Using the following equation, the error estimate is calculated.

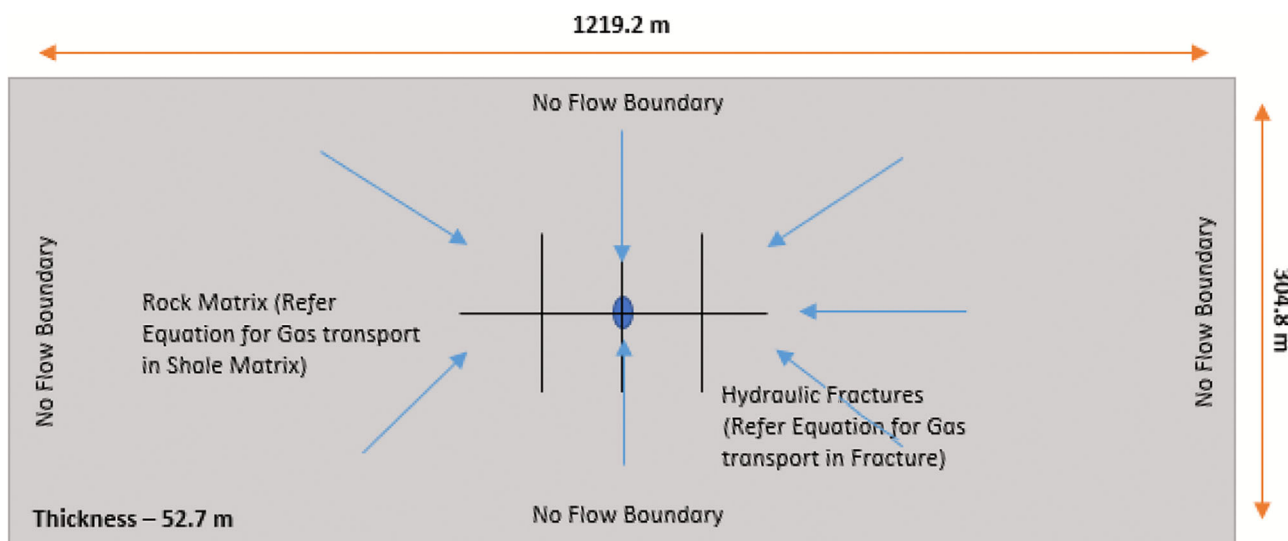


FIGURE 3 Schematic of base model for parametric investigation of reservoir characteristics.

When the error estimate is small enough, this model is then converged.

$$\rho |M^{-1}(b - Ax)| < \text{tol.} |M^{-1}b| \quad (23)$$

The iterations end when the relative (preconditioned) residual times the factor ρ is less than a tolerance tol , according to the Equation (22) convergence criterion. If the system matrix A is ill-conditioned, the iterations for solvers where M is equal to the identity matrix may occasionally end too soon and produce the wrong answer. If M is a weak preconditioner, the iterations for solvers where M is not equal to the identity matrix may occasionally end too soon. Increase the factor ρ to a number of the order of the condition number for the matrix $M^{-1}A$ if the iterations end too soon because of an ill-conditioned system matrix or a subpar preconditioner. The convergence criterion indicates that the relative error is less than tol if ρ is and more significant than the condition number for the matrix $|M^{-1}(b - Ax)| < \text{tol.} |M^{-1}b|$.

TABLE 1 Reservoir parameters for the base model.

Reservoir parameters	Values	Units
Langmuir pressure	3×10^6	Pa
Langmuir volume	2.5×10^{-3}	m^3/kg
Initial reservoir pressure	34.5×10^6	Pa
Bottom hole pressure	2.4×10^6	Pa
Reservoir temperature	352	K
Hydraulic fracture width	0.003	m
Initial fracture permeability	30	mD
Hydraulic fracture spacing	30.5	m
Hydraulic fracture half-length	85.3	m
Number of fractures	14	-
Initial matrix permeability	1×10^{-19}	m^2
Initial fracture porosity	0.03	-
Possion's ratio	0.2	-
Matrix permeability	0.021	-

TABLE 2 Summary of observable results based on different mesh sizes.

Cases	In-built type	Maximum element size	Minimum element size	Maximum element growth rate	Curvature factor	Resolution of narrow regions
Case 1	Fine	10.6	0.06	1.3	20	1
Case 2	Normal	13.4	0.06	1.3	0.4	1
Case 3	Coarse	20	0.4	1.4	1.4	1
Case 4	Coarser	66	10	2	2	0.9

3 | DISCUSSION AND RESULTS

3.1 | Model validation

Model validation uses real-field data from Marcellus shale gas production.^[16] Different studies utilize this data as a benchmark due to its availability, and various other shale models can also represent it. Table 2 provides the required parameters to validate the gas transport model. Compared to the study of Micheal et al.,^[16] which followed similar validation, geomechanical influence is ignored due to a slight error in the production profiles. Figure 4 depicts that the gas transport model is in good agreement with the real-field data, with a maximum error of up to 9%, which is expected due to certain assumptions made with the model.^[16]

A good agreement is observed between the validation model and Marcellus Shale's historical data. The gas production rate decreases from $9 \times 10^4 \text{ m}^3/\text{day}$ to $3.7 \times 10^4 \text{ m}^3/\text{day}$ over 250 days. The errors observed can be attributed to the heterogeneity of the shale formation. Micheal et al.^[16] proposed a quadruple continuum model, providing a similar outcome. Cao et al.^[5] also utilized Marcellus shale historical data and also had a good agreement. There are inconsistencies in the validation model as it did not show much influence from the adsorption characteristics.^[5]

An additional parametric study was conducted to define different parameters for further parametric study through DCA to validate it. It is observed that Langmuir volume depicted negligible influence on the cumulative production as examined in other studies.^[16,52]

3.2 | Production results of base case model and study of fracture characteristics

Figure 5 depicts the production performance of the base case model based on the parameters mentioned in Table 1. The production declines rapidly from $383216.7 \text{ m}^3/\text{day}$ to $114470.3 \text{ m}^3/\text{day}$, which is justified by similar trends observed in historical performance

FIGURE 4 Mesh sensitivity.

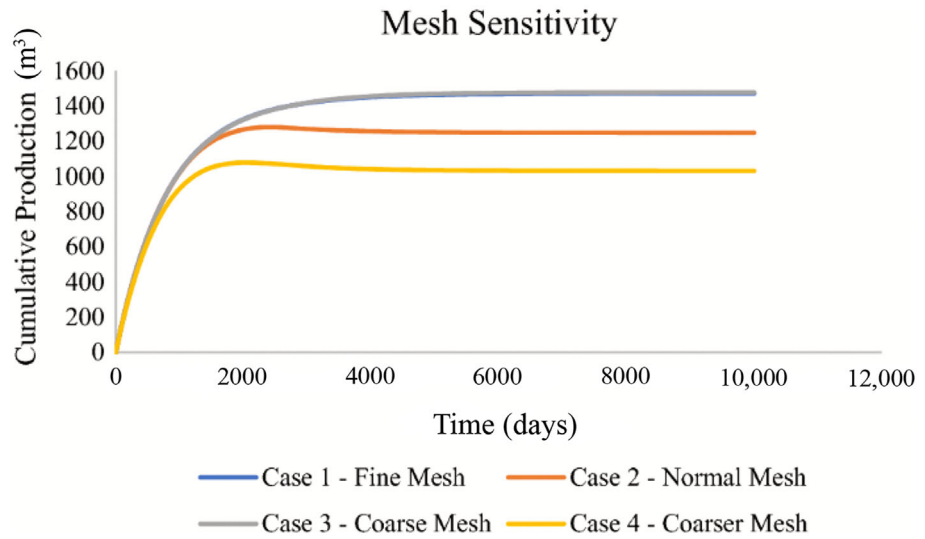


FIGURE 5 Historical data of Marcellus shale and validation model.

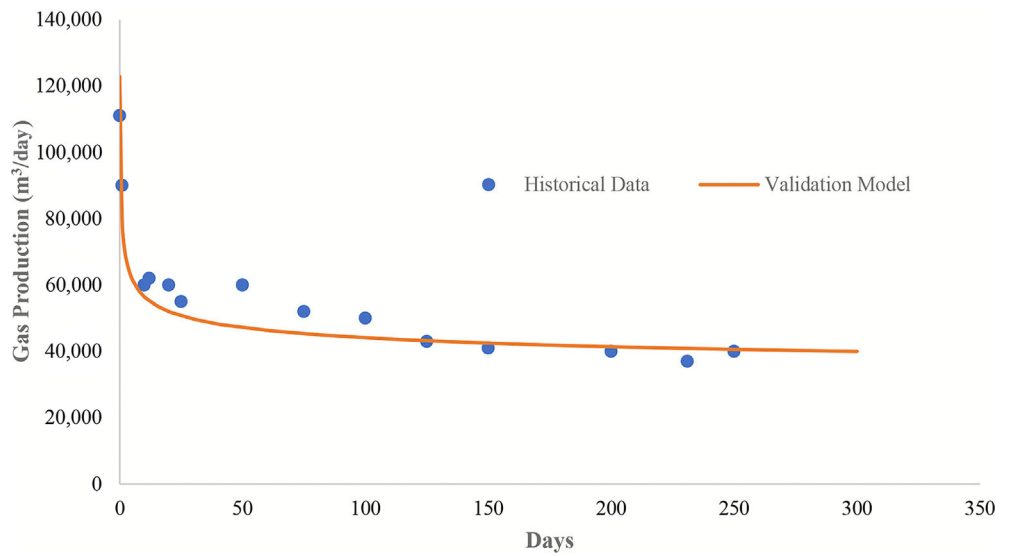
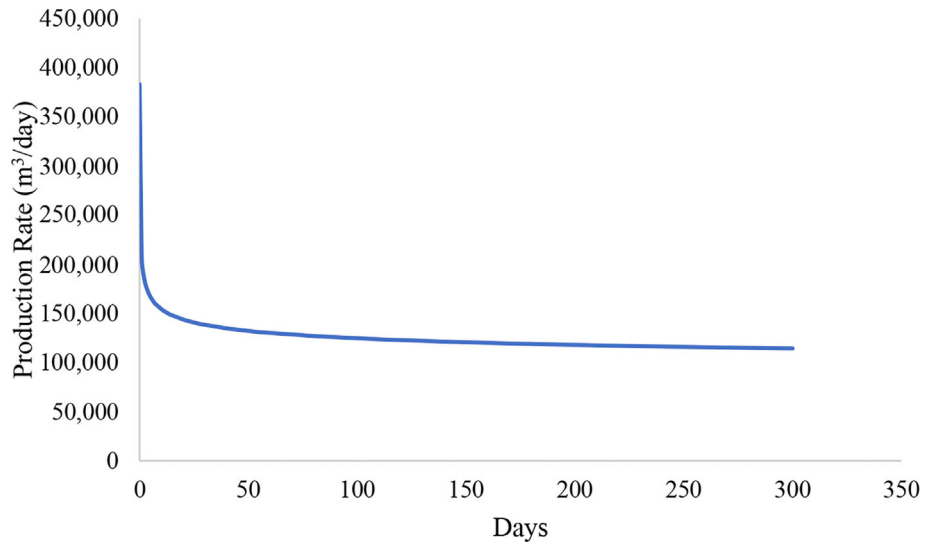


FIGURE 6 Production performance of base case model.



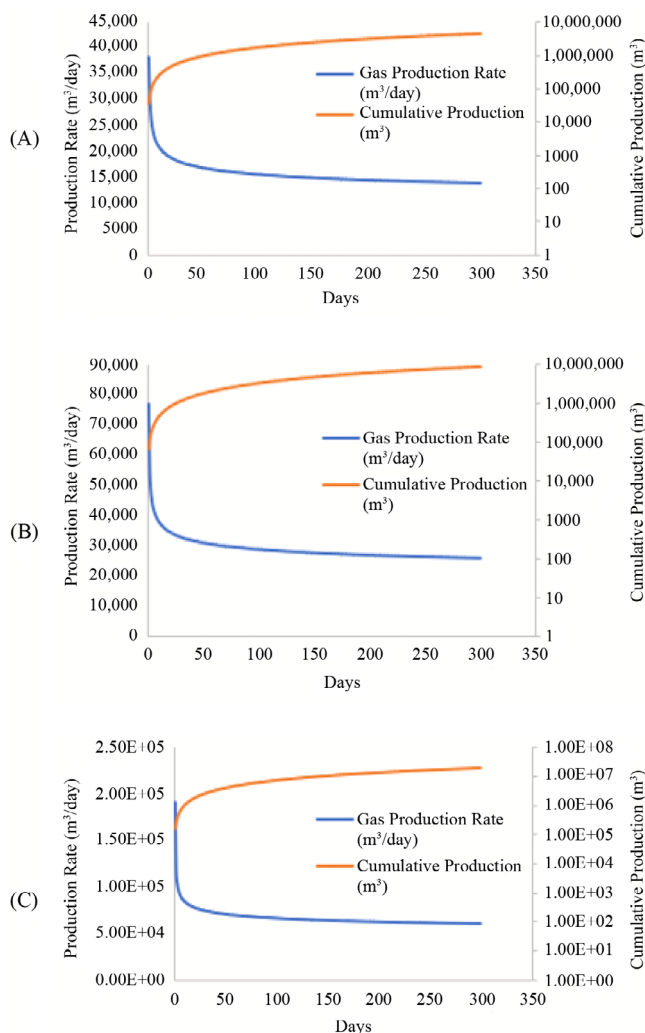


FIGURE 7 (A) Production performance of hypothetical during fracture permeability of 10 mD; (B) Production performance during fracture permeability of 20 mD; (C) Production performance during fracture permeability of 50 mD.

data from shale gas, reservoirs, and other SGTMs.^[17,21,50,56] In this case, the gas phase influencing the production performance was free gas content in the matrix. The free gas diffuses into the hydraulic fractures and then to the wellbore. For this particular study, hydraulic fractures are considered from a horizontal well.

The trends observed in Figures 6 and 7 are similar to other complex reservoirs with an initial production spike and fast dying-out rate due to lower reservoir energy. These formations generally have lower production energy due to inadequate flow channels. Additional analysis is done to determine the reservoir's fracture characteristics that can influence production. Fracture porosity and fracture permeability were selected for the parametric analysis using DCA. Figures 6 and 7 represent different production profiles corresponding to different fracture porosities and

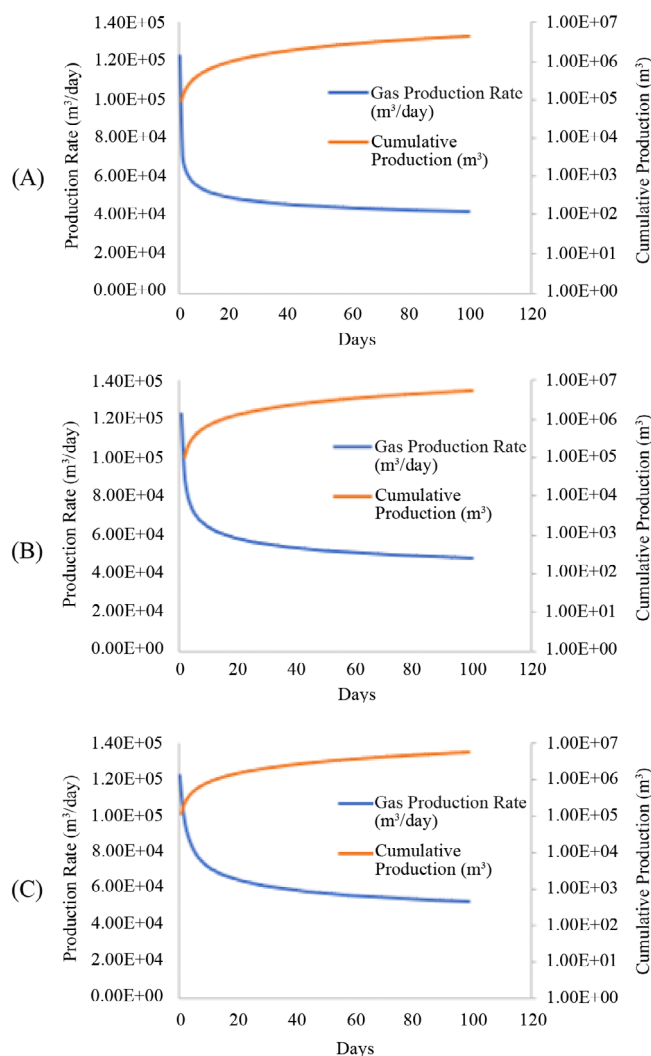


FIGURE 8 (A) Production performance of hypothetical during fracture porosity of 0.01; (B) Production performance during fracture porosity of 0.05; (C) Production performance during fracture porosity of 0.12.

permeabilities. With an increase in fracture porosity and permeability, there is a resulting increase in the production rates and decline rates. The objective is to obtain similar trends during the production data analysis of these scenarios. The fracture permeability has a more significant influence on the production rate of the reservoir than the porosity. A similar ratio of increase between the parameters of the fracture domain and gas production performance is observed; however, doubling the permeability of the reservoir results in a doubling of the production rate (32,772 to 65,544 m³/day). Other parameters such as adsorption/desorption, matrix properties, and temperature change have not been studied in this work as the purpose was to propose a novel method of coupling CFD for reservoir modeling to DCA for reserve estimation.

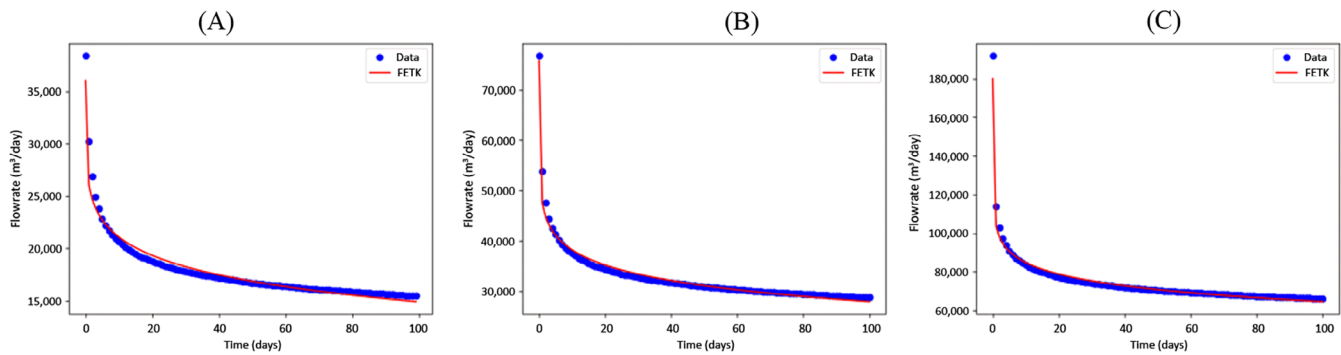


FIGURE 9 Curve fitting and prediction of production using exponential decline curve analysis (EDCA) for fracture permeabilities of (A) 10 mD; (B) 20 mD; (C) 50 mD (where FETK refers to predicted data from the model).

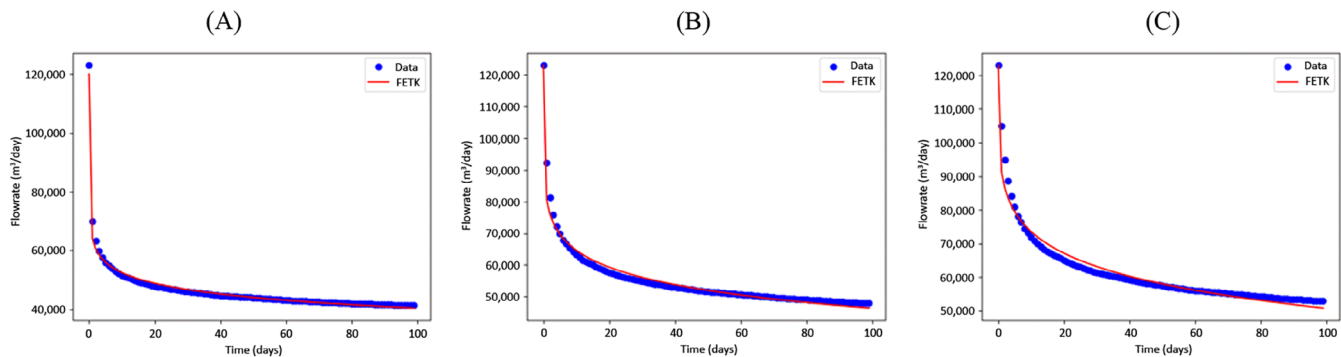


FIGURE 10 Curve fitting and prediction of production using exponential decline curve analysis (EDCA) for fracture porosities of (A) 1%; (B) 5%; (C) 12% mD (where FETK refers predicted data from the model).

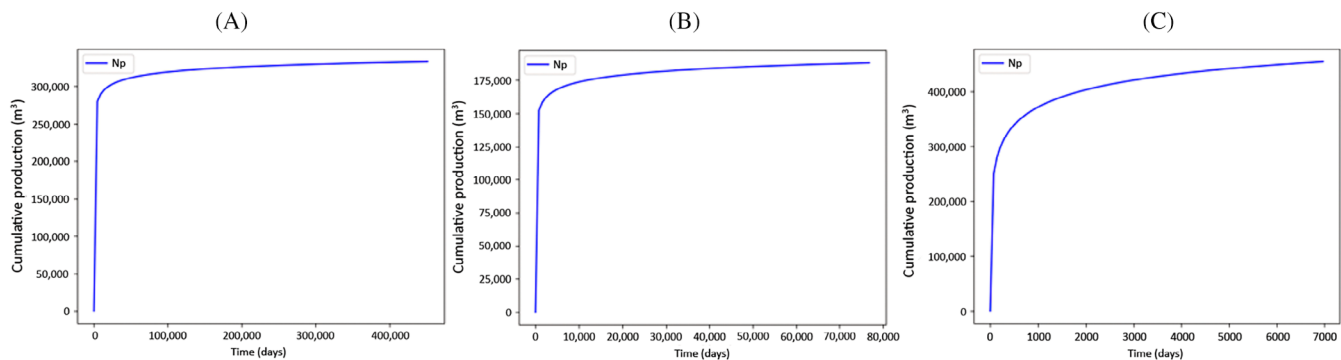


FIGURE 11 Total recoverable reserves up to economic limit for fracture permeabilities of (A)10 mD; (B) 20 mD; (C) 50 mD.

3.3 | Estimation of recoverable reserves

A Python model is developed for curve-fitting to obtain the DCA parameters for the forecasting. As mentioned earlier, forecasting is required to determine the production when it reaches an economic limit. In this study, the economic limit is capped at 10,000 m³/day to eradicate any errors or complexity in the results. Nevertheless, it can be reduced to a reasonable rate after a comprehensive economic analysis. This analysis aims to validate and

predict the recoverable reserves and the influence of variation of reservoir characteristics. Initially, there was a minor change in the variation of Langmuir volume due to its lower volume in this study; therefore, adsorbed gas still needs to be studied. However, with other shale gas reservoirs, it is essential to note that Langmuir volume is the defining characteristic of estimating adsorbed gas and would have a higher impact.

Figures 8 and 9 represent the curve-fitting process to determine the decline parameters that will be utilized

for forecasting. Figures 10 and 11 represent different production forecasts obtained using the Arps model, while Table 3 includes different decline curve parameters obtained. A Python model is implemented to make it easy to determine them (the source code utilized for this purpose is in the Data S1).

Table 4 shows that with the increase in initial fracture permeability and porosity, there is a significant increase in recoverable reserves. However, with the increase in

permeability, the decline rate decreases, while the increase in porosity causes the decline rate to increase. This decline is also represented in the days required to reach the assumed economic limit for this study (10,000 m³/day).

Based on the results observed in Table 4 and Figures 10 and 11, it can be determined that DCA can also be utilized for complex reservoirs. However, additional validation with reservoir volumetric data is further required. Section the validation that was done in Section 3.1 based solely on the production data observed from Marcellus shale. Further, the model was limited to the dimensions assumed, which was why these results were observed. It is to be noted that the fitting of the DCA model itself is a proof of concept that it can be utilized for these types of reservoirs. Additionally, future work can include correcting the under or over-predictions of DCA for complex reservoirs. The complexity of these unconventional reservoirs arises from comprising more than a single domain of fluid flow (matrix and fracture) and more than a single flow mechanism (diffusion and desorption).^[16,57,58] The study thus can be an initial step in the easement of quantification of reserves for complex reservoirs using conventional means—DCA (Table 5).

Additional uncertainties observed during the study included variations in results due to variations in the fracture properties, as shown in Figures 10 and 11. The assumed model properties, such as isothermal field life, restricted any uncertainties in the observed result; however, while dealing with the non-isothermal model, SGTM must be modified to account for the variations (Figure 12).

TABLE 3 Reservoir parameters for validation model.

Parameters	Marcellus shale	Units
Reservoir dimension	1219.2 × 304.8 × 52.7	m ³
Langmuir pressure	3 × 10 ⁶	Pa
Langmuir volume	2.5 × 10 ⁻³	m ³ /kg
Initial reservoir pressure	34.5 × 10 ⁶	Pa
Bottom hole pressure	2.4 × 10 ⁶	Pa
Reservoir temperature	352	K
Gas viscosity	2 × 10 ⁻⁵	m · s
Hydraulic fracture width	0.003	m
Initial fracture permeability	30	mD
Hydraulic fracture spacing	30.5	m
Hydraulic fracture half-length	85.3	m
Number of fractures	14	-
Initial matrix permeability	1 × 10 ⁻¹⁹	m ²
Initial fracture porosity	0.03	-
Possion's ratio	0.2	-

TABLE 4 Obtained fitting parameters through exponential decline curve analysis (EDCA).

Parameters	Symbols	Units	Fracture permeability			Fracture porosity		
			10 mD	20 mD	50 mD	0.01	0.05	0.12
Initial production rate	q_i	m ³ /d	38,401	76,772	192,500	122,700	122,860	122,930
Decline exponent parameter	b	-	0.22	0.16	0.13	0.12	0.18	0.24
Nominal decline rate	D_i	1/day	0.33	0.47	0.55	0.63	0.42	0.30

TABLE 5 Recoverable reserves based on variations of reservoir characteristics.

Reserve estimation results	Units	Fracture permeability			Fracture porosity		
		10 mD	20 mD	50 mD	0.01	0.05	0.12
Days to reach economic limit	days	594.85	8416	451,290	76,836	9654.2	6970
Total recoverable reserves	m ³	83120.31	156,031	333,238	188,039	349,166	454,785

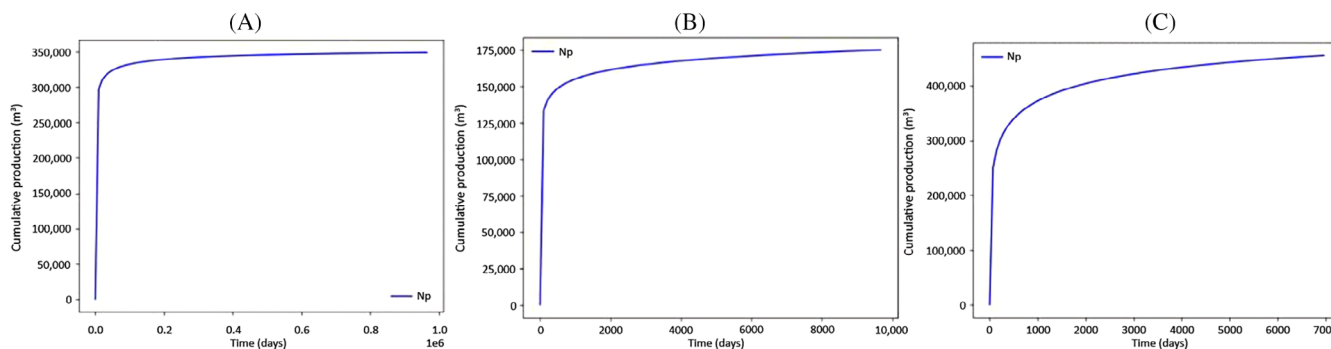


FIGURE 12 Total recoverable reserves until economic limit of 10,000 m³/day for fracture porosities of (A) 0.01; (B) 0.05; (C) 0.12.

4 | CONCLUSION

This study introduces an innovative approach combining DCA with SGTm, aiming to optimize performance evaluation and characterize reservoirs. Unlike traditional market-available reservoir simulation tools, our methodology integrates intricate flow mechanisms into SGTm, offering insights into production dynamics and total recoverable reserves. This integration holds promise for enhancing field development planning of unconventional shale gas reservoirs.

Key advantages of our outlined methodology include:

- Reduced computational cost and time: Leveraging the COMSOL Multiphysics software enables efficient modelling and simulation of shale gas transport with minimal input parameters.
- Accurate representation of transport mechanisms: Incorporating a dual porosity and DP model for the matrix alongside a linear flow model for fractures accounts for complex shale gas transport mechanisms and dispersed kerogen distribution.
- Reliable reserves estimation: Utilizing exponential DCA based on production data from the reservoir model ensures dependable reserves estimation.
- While EDCA serves as the foundation of this study, we acknowledge the potential for incorporating additional methods and alternative production data analysis techniques. Through this methodology, reservoir simulations conducted via CFD tools facilitate the implementation of diverse complex flow mechanisms, aiding in the estimation of recoverable reserves.

Recommendations for future research prospects include:

- Benchmarking with conventional simulation software: Validating our results against established reservoir simulation software.

- Exploration of alternate transport models: Employing alternative SGTm with higher degrees of freedom for enhanced sensitivity analysis.
- Comparative analysis with other complex reservoir data: Benchmarking our findings against diverse reservoir datasets.
- Refinement of DCA models: Correcting DCA models based on reservoir geological data, including matrix and fracture properties.

AUTHOR CONTRIBUTIONS

Syed Oubei Khadri: Conceptualization; data curation; formal analysis; writing – original draft; software; validation; methodology. **Mohammed J. Al-Marri:** Conceptualization; writing – original draft; methodology; writing – review and editing. **Mustafa Nasser:** Conceptualization; writing – original draft; methodology; funding acquisition; writing – review and editing. **Fadhil Sadooni:** Conceptualization; writing – original draft; writing – review and editing; supervision; funding acquisition. **Ezeddin Shirif:** Conceptualization; methodology; formal analysis; writing – review and editing; validation. **Ibnelwaleed A. Hussein:** Conceptualization; funding acquisition; supervision; project administration; writing – review and editing; formal analysis.

ACKNOWLEDGEMENTS

The authors would like to acknowledge the support of the Qatar National Research Fund (a member of the Qatar Foundation) through Grant NPRP12S-0130-190023 and NPRP12S-0305-190235. The findings achieved herein are solely the responsibility of the authors. Qatar University Open Access publishing facilitated by the Qatar National Library, as part of the Wiley Qatar National Library agreement.

PEER REVIEW

The peer review history for this article is available at <https://www.webofscience.com/api/gateway/wos/peer-review/10.1002/cjce.25359>.

DATA AVAILABILITY STATEMENT

The data that support the findings of this study are available upon request from the corresponding author. The data are not publicly available due to privacy or ethical restrictions.

ORCID

Ibnelwaleed A. Hussein  <https://orcid.org/0000-0002-6672-8649>

REFERENCES

- [1] W. Shen, X. Li, Y. Xu, Y. Sun, W. Huang, *Energies* **2017**, *10*, 751.
- [2] K. Liu, M. Ostadhassan, J. Zhou, T. Gentzis, R. Rezaee, *Fuel* **2017**, *209*, 567.
- [3] H. Wang, L. Chen, Z. Qu, Y. Yin, Q. Kang, B. Yu, W. Q. Tao, *Appl. Energy* **2020**, *262*, 114575.
- [4] H. Zhang, W. Peng, P. Hao, M. du, *Int. J. Oil, Gas Coal Technol.* **2019**, *20*, 397.
- [5] P. Cao, J. Liu, Y. K. Leong, *Fuel* **2016**, *178*, 103.
- [6] C. M. Freeman, G. J. Moridis, T. A. Blasingame, *Transp. Porous Media* **2011**, *90*, 253.
- [7] L. Liang, D. Luo, X. Liu, J. Xiong, *J. Nat. Gas Sci. Eng.* **2016**, *33*, 1107.
- [8] L. Wang, A. Torres, L. Xiang, X. Fei, A. Naido, W. Wu, *Nat. Resour.* **2015**, *06*, 141.
- [9] S. Zendejboudi, *Shale Oil and Gas Handbook*, Elsevier, Houston, TX **2017**.
- [10] Y. Liu, L. Liu, J. Y. Leung, K. Wu, G. Moridis, *SPE J.* **2021**, *26*, 1.
- [11] D. S. Berawala, P. Andersen, *J. Pet. Sci. Eng.* **2020**, *190*, 107114.
- [12] M. B. Asadi, M. Dejam, S. Zendejboudi, *J. Hydrol.* **2020**, *581*, 124288.
- [13] C. M. Freeman, G. Moridis, D. Ilk, T. A. Blasingame, *J. Pet. Sci. Eng.* **2013**, *108*, 22.
- [14] W. Zhang, W. Chen, T. Wang, Y. Yang, *J. Nat. Gas Sci. Eng.* **2020**, *81*, 103471.
- [15] Y. Zhao, C. Wang, J. Bi, *Energy Science and Engineering* **2020**, *8*, 1220.
- [16] M. Micheal, W. L. Xu, H. Y. Xu, J. N. Zhang, H. J. Jin, H. Yu, H. A. Wu, *J. Nat. Gas Sci. Eng.* **2021**, *95*, 104156.
- [17] L. Tan, L. Zuo, B. Wang, *Energies* **2018b**, *11*, 552.
- [18] S. Coutry, M. Tantawy, S. Fadel, *J. Eng. Appl. Sci.* **2023**, *70*, 69.
- [19] P. Thararoop, Z. T. Karpyn, T. Ertekin, *J. Nat. Gas Sci. Eng.* **2012**, *8*, 121.
- [20] O. Vorobiev, T. Antoun, *International Journal for Numerical Methods in Engineering* **2011**, *86*, 1101.
- [21] D. Y. Ding, N. Farah, B. Bourbiaux, Y. S. S. Wu, I. Mestiri, *SPE J.* **2018**, *23*, 1389.
- [22] T. Zhang, S. Sun, H. Song, *Transp. Porous Media* **2019**, *126*, 655.
- [23] F. Civan, C. S. S. Rai, C. H. H. Sondergeld, *SPE J.* **2012**, *17*, 717.
- [24] D. Chai, X. Li, presented at the SPE Western Regional Meeting, Virtual. April **2021**.
- [25] Q. Gao, S. Han, Y. Cheng, X. Shi, C. Yan, Z. Han, *Energy* **2022**, *257*, 124727.
- [26] K. Wu, X. Li, C. Wang, W. Yu, Z. Chen, presented at the SPE/CSUR Unconventional Resources Conf, Calgary, AB, Canada. October **2015**.
- [27] J. Zeng, J. Liu, J. Guo, *Chem. Eng. J.* **2022**, *438*, 135604.
- [28] C. Guo, M. Wei, H. Liu, *PLoS One* **2015**, *10*, 1.
- [29] S. A. Abubakar, S. Mori, J. Sumner, *Metals* **2022**, *12*, 1397.
- [30] L. Germanou, M. T. Ho, Y. Zhang, L. Wu, *J. Nat. Gas Sci. Eng.* **2018**, *60*, 271.
- [31] W. Guo, X. Zhang, R. Yu, L. Kang, J. Gao, Y. Liu, *Frontiers in Earth Science* **2022**, *9*, 1.
- [32] Y. Li, A. Kalantari-Dahaghi, A. Zolfaghari, P. Dong, S. Negahban, D. Zhou, *Int. J. Heat Mass Transfer* **2020**, *148*, 119026.
- [33] L. Geng, G. Li, S. Tian, M. Sheng, W. Ren, P. Zitha, *AIChE J.* **2017**, *63*, 1430.
- [34] L. Zhang, K. Wu, Z. Chen, X. Yu, J. Li, S. Yang, G. Hui, M. Yang, *Planet. Space Sci.* **2021**, *204*, 105283.
- [35] F. Tian, X. Luo, W. Zhang, *Mar. Pet. Geol.* **2019**, *99*, 292.
- [36] H. Yin, J. Zhou, X. Xian, Y. Jiang, Z. Lu, J. Tan, G. Liu, *Energy* **2017**, *132*, 84.
- [37] F. Du, B. Nojabaei, *Energies* **2019**, *12*, 2355.
- [38] C. W. Neil, M. Mehana, R. P. Hjelm, M. E. Hawley, E. B. Watkins, Y. Mao, H. Viswanathan, Q. Kang, H. Xu, *Communications Earth & Environment* **2020**, *1*, 49.
- [39] K. Wu, Z. Chen, X. Li, *Chem. Eng. J.* **2015**, *281*, 813.
- [40] M. Mahmoud, *J. Energy Resour. Technol.* **2014**, *136*, 012903.
- [41] A. L. Lee, M. H. Gonzalez, B. E. Eakin, *J. Pet. Technol.* **1966**, *18*, 997.
- [42] Z. Jiang, W. Wang, H. Zhu, Y. Yin, Z. Qu, *Energy Fuels* **2023**, *37*, 2520.
- [43] R. Cui, S. M. Hassanizadeh, S. Sun, *Earth-Sci. Rev.* **2022**, *234*, 104203.
- [44] Z. Jin, A. Firoozabadi, *Fluid Phase Equilib.* **2014**, *382*, 10.
- [45] D. J. K. Ross, R. Marc Bustin, *Mar. Pet. Geol.* **2009**, *26*, 916.
- [46] S. Zhan, Y. Su, M. Lu, M. Cai, J. Fu, Z. Liu, K. Wang, Q. Han, *Geofluids* **2021**, *2021*, 1.
- [47] C. Afagwu, M. A. Mahmoud, S. Alafnan, S. Patil, *J. Pet. Sci. Eng.* **2022**, *208*, 109518.
- [48] J. E. Warren, P. J. Root, *Soc. Pet. Eng. J.* **1963**, *3*, 245.
- [49] K. Guo, B. Zhang, K. Aleklett, M. Höök, *Sustainability* **2016**, *8*, 973.
- [50] H. Zhang, D. Rietz, A. Cagle, M. Cocco, J. Lee, *J. Nat. Gas Sci. Eng.* **2016**, *36*, 402.
- [51] H. Tang, B. Zhang, S. Liu, H. Li, D. Huo, Y. S. Wu, *J. Nat. Gas Sci. Eng.* **2021**, *88*, 103818.
- [52] C. Guo, M. Wei, H. Liu, *PLoS One* **2018**, *13*, 1.
- [53] B. Hu, J. G. Wang, K. Zhang, Z. Ye, *J. Nat. Gas Sci. Eng.* **2020**, *78*, 103335.
- [54] Y. Lu, S. Wei, Y. Xia, Y. Jin, *J. Pet. Sci. Eng.* **2021**, *196*, 107576.
- [55] W. Yu, K. Sepehrnoori, T. W. Patzek, presented at the SPE Annual Technical Conf and Exhibition, Amsterdam, The Netherlands. October **2014**.
- [56] K. Wang, B. Jiang, H. Li, Q. Liu, C. Bu, Z. Wang, Y. Tan, *Int. J. Coal Geol.* **2020**, *218*, 103359.
- [57] F. Aminzadeh, S. N. Dasgupta, *Dev. Pet. Sci.* **2013**, *60*, 247.

- [58] A. Vafaie, I. R. Kivi, S. A. Moallemi, B. Habibnia, *Unconventional Resources* **2021**, *1*, 9.

SUPPORTING INFORMATION

Additional supporting information can be found online in the Supporting Information section at the end of this article.

How to cite this article: S. O. Khadri, M. J. Al-Marri, M. Nasser, F. Sadooni, E. Shirif, I. A. Hussein, *Can. J. Chem. Eng.* **2024**, *1*. <https://doi.org/10.1002/cjce.25359>